# Electrical tuning of helical edge states in topological multilayers

T. Campos<sup>1,4</sup>, M. A. Toloza Sandoval<sup>2</sup>, L. Diago-Cisneros<sup>3,4</sup>, G. M. Sipahi<sup>4</sup>

- $^{\rm 1}$  Department of Physics, State University of New York at Buffalo, Buffalo, New York 14260, USA
- <sup>2</sup> Instituto de Física, Universidade Federal da Bahia, Salvador, Bahia 40210-340, Brazil.
- $^3$  Facultad de Física, Universidad de La Habana, La Habana 10400, Cuba
- $^4$ Instituto de Física de São Carlos, Universidade de São Paulo, São Carlos, São Paulo 13566-590, Brazil

Abstract. Mainstream among topological insulators, GaSb/InAs quantum wells present a broken gap alignment for the energy bands which supports the quantum spin Hall insulator phase and forms an important building block in the search of exotic states of matter. Such structures allow the band-gap inversion with electrons and holes confined in adjacent layers, providing a fertile ground to tune the corresponding topological properties. Using a full 3D 8-band  $\mathbf{k}\cdot\mathbf{p}$ method we investigate the inverted band structure of GaSb/InAs/GaSb and InAs/GaSb/InAs multilayers and the behavior of the helical edge states, under the influence of an electric field applied along the growth direction. By tuning the electric field modulus, we induce the change of the energy levels of both conduction and valence bands, resulting in a quantum spin Hall insulator phase where the helical edge states are predominantly confined in the GaSb layer. In particular, we found that InAs/GaSb/InAs has a large hybridization gap of about 12 meV and, therefore, are promising to observe massless Dirac fermions with a large Fermi velocity. Our comprehensive characterization of GaSb/InAs multilayers creates a basis platform upon which further optimization of III-V heterostructures can be contrasted.

## 1. Introduction

Conducting edge states are key pieces to understand the conceptual puzzle behind the topological phases of matter [1, 2]. Remarkably, unlike the integer quantum Hall phase, which can be basically understood in terms of chiral edge modes, quantum spin Hall insulators host time-reversal protected helical edge states connecting valence and conduction bulk bands - the former case is fundamentally different from the latter due to the presence of an external magnetic field that breaks the time-reversal symmetry. Nevertheless. the spin Hall insulator phase was experimentally observed, in InAs/GaSb and HgTe/(Hg,Cd)Te based heterostructures, even for high magnetic fields [3, 4], and such unexpected robustness of the gapless (edge) states forms a recent topic of discussions [5, 6, 7].

Over decades InAs/GaSb based structures have attracted much attention in view of their unique properties, since the seminal works exploring their unconventional band alignment [8, 9], where the top of the GaSb valence band is higher than the bottom of the InAs conduction band, forming a broken gap at the interface. In especial, such broken gap alignment allows the collapse of the energy gap with electrons and holes confined in adjacent layers, providing a fertile testing-ground for fundamental and applied condensed matter physics [10, 11, 12, 13, 14, 15, 16]. After a striking prediction [17], the quantum spin Hall insulator phase was experimentally observed in InAs/GaSb heterostructures by different groups [3, 18, 19, 20, 21, 22, inspiring a race in the search of different exotic phases of matter [7, 23, 24, 25, 26, 27, 28, 29].

Nowadays, there is a plethora of reports characterizing the edge conductance behavior of InAs/GaSb asymmetric quantum well (AQW) [3, 18, 19, 20, 21, 22, 26, 27, 28, 30, 31, 32, 33, 34, 35, 36]. Furthermore, electrical control of the topological phase transition is possible [37, 38, 39] and has been reported for InAs/GaSb AQWs [6, 40, 41, 42, 43]. Although very recently Krishtopenko and Teppe [7] proposed that threelayer InAs/GaSb quantum well (QWs) hosts topological phase transition, their focus was on the strain engineering of the band gap of the InAs/GaInSb QWs which they claim is of the order of 60 meV. Instead, we focus on the electrical control, of the phase transition and the behavior of the helical edge states in such three-layer QWs, using an applied electric field but neglecting e-e interaction and disorder effects.

In one hand, the helical edges states with hidden Dirac point constitute a possible explanation for the aforementioned robustness, on the other, they are described as massless Dirac fermions with an exactly linear dispersion only in the vicinity of the Dirac point (or small k). Additionally, we also show that it is possible to tune the inverted-band structure aiming to obtain massless Dirac fermions with a large fermion velocity. In order to make this evaluation, we use a full 3D 8-band  $\mathbf{k} \cdot \mathbf{p}$  method [44, 45, 46, 47, 48] and employ the envelope function approximation to take into account the quantum confinement [46, 49], together with the plane wave expansion [50, 51]. In this way, we were capable to have a full three dimensional solution of the system which is specially important to analyze, for example, the spatial distribution of the helical edge states along the confinement profile.

In the inverted band regime the hybridization gap,  $\Delta E_h$ , is opened at a finite wave vector,  $k_c$ , with Fermi velocity  $v_F \approx \frac{\Delta E_h}{2\hbar k_c}$  [28, 42]. By changing the layer size and/or applying an external electric field, the value of  $k_c$  and  $\Delta E_h$  can be tuned. Usually, low values of  $k_c$  (higher of  $v_F$ ) are desired such that the bulk states do not coexist with the edge Hence, a system where  $k_c$  is as close as possible to the  $\Gamma$ -point and the  $\Delta E_h$  is as large as possible, minimizes all the rich yet undesired physical phenomena that interferes with the edge states [23, 24, 25, 27, 29]. The estimation of the wave vector values in which the hybridization occurs gives the range  $k_c \in [0.1, 0.3] \,\mathrm{nm}^{-1}$  suggesting that the systems are in the deeply inverted regime [28]. Moreover, both InAs/GaSb AQWs and GaSb/InAs/GaSb symmetric quantum wells (SQWs) have similar hybridization gaps,  $\Delta E_h \approx 5 \,\mathrm{meV}$ , leading to similar low values of Fermi velocity  $v_F \in [1,4] \times 10^4 \,\mathrm{ms}^{-1}$  while InAs/GaSb/InAs SQWs have  $v_F \in [3, 9] \times 10^4 \,\mathrm{ms}^{-1}$ ,  $\Delta E_h \approx 12 \,\mathrm{meV}$  suggesting that InAs/GaSb/InAs SQWs should be a better candidate to host massless Dirac fermions.

In summary, the race to build reliable platforms where the properties of the topological phase can be efficiently harnessed is still on. One among several possible applications is to build devices where Majorana fermions could be easily braided [52, 53]. Moreover, very recently it was shown that the hybridization gap of InAs/GaSb/InAs multilayers is temperature independent [54] and also a clear evidence of the massless Dirac fermions was reported [55].

Our main motivation and purpose is to demonstrate the possibility to tune multilayers as those depicted in figure 1 into a topological regime by applying an electric field, and this way enabling topological-edge states to arise. The theoretical modeling we present highlights the relevance of InAs/GaSb three-layer heterostructure for searching new topological phase transitions, due to the intrinsic alignment of quasi-bound electron states to quasi-bound hole levels as needed. We hope that our study could be used as a guidance in order to develop novel devices that use switchable topological phase transitions.

# 2. Topological Broken-Gap Multilayers

In this manuscript we study two distinct arrangements of broken-gap multilayers that present topological features. The first system, GaSb/InAs/GaSb, consists of one InAs layer surrounded by two GaSb layers, see figure 1(a)-(b), and does not present a hybridization The application of an external electric field induces a Rashba spin-orbit coupling (SOC) that yields a hybridization gap that, as we will show, have values close to the ones of a regular AQW of about 5 meV. In the second system, InAs/GaSb/InAs, consisting of one GaSb layer surrounded by two InAs layers, see figure 1(c)-(d), there is an anticrossing of the electron and heavy-hole bands but no overall gap (see Supplementary Material). When an electric field is applied the system now shows a hybridization gap of the order of 12 meV that is stable under changes of the applied electric field.

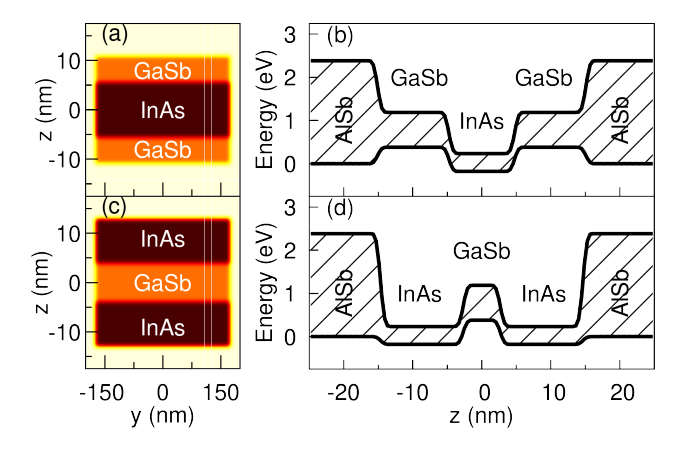


Figure 1. Confinement profile of the broken-gap multilayers. (a) and (b) slab configuration with quantum confinement along both y and z directions and quantum well confinement profile for the InAs/GaSb/InAs multilayer system; (c) and (d) slab configuration and quantum well confinement profile for the GaSb/InAs/GaSb multilayer system.

Although the existence of the hybridization gap is important for these systems, its is only effective when this gap results in an overall gap, *i. e.*, that stands for

all k points, appearing as a general feature in the DOS of the system. For both configurations we analyze how the hybridization gap changes when Rashba SOC is controlled by the external electric field, directly tuning the values of the overall density of states (DOS) gap. We also analyze the quantum spin Hall phase when we turn the system from a quantum well into a slab, by adding a weak quantum confinement along one of the previous free directions. In figure 1 we depicted the confinement profile of both cases, quantum well and slab configuration.

The energies of the states can be tuned by changing the layer sizes. By changing them it may be possible to align quasi-bound electron states of InAs to quasi-bound hole levels of the GaSb, leading to conditions for resonance tunneling or even giant conductance regime [56]. Moreover, as the effective masses of electrons are much smaller than the holes' counterparts, this tuning may be done more effectively by changing the sizes of the InAs layer  $(L_{InAs})$ . Carefully adjusting the layers sizes of the GaSb layers  $(L_{\text{GaSb}})$  the hole's energy can cross the electron's one and the system may be driven from an insulating phase to a band inverted phase [7, 57, 58]. In the rest of this article we explore the regimes in which such energy level crossings leads to a topological phase transition by tuning the applied electric field.

## 2.1. GaSb/InAs/GaSb multilayer

The confinement profile of the GaSb/InAs/GaSb system leads to a spatial separation of the carriers as seen in figure 1(b), electrons being confined in the InAs layer and holes in the GaSb layers. Without breaking the system inversion symmetry, the GaSb/InAs/GaSb SQW will only have a semiconductor-semimetal transition, as discussed in the Supplementary Material.

Heatmaps showing the overall gap as a function of the  $L_{\rm InAs}$  and  $L_{\rm GaSb}$  are shown in figure 2(a)-(c) for three different absolute values of the electric field  $|E|=1\,{\rm mV\,nm^{-1}},\ |E|=3\,{\rm mV\,nm^{-1}}$  and  $E=|5|\,{\rm mV\,nm^{-1}}$ . Two different trends may be extracted from these graphics. First, if the size of one layer and of the electric field are fixed, the variation of the size of the other layer induces a threshold in which the hybridization gap opens. Further increasing the size of this layer, the gap reaches a maximum and decays up to a second threshold where the gap closes, forming a crescent moon shape. Second, if the applied electric field value is increased, the initial thresholds are moved to smaller values of  $L_{\rm InAs}$  and  $L_{\rm GaSb}$  and the gaped region is compressed when  $L_{\rm InAs} \approx L_{\rm GaSb}$  and stretched when they are more separated.

Both behaviors can be explained with a simple argument. The electric field ramp changes the band edges differently for each layer and, consequently, also

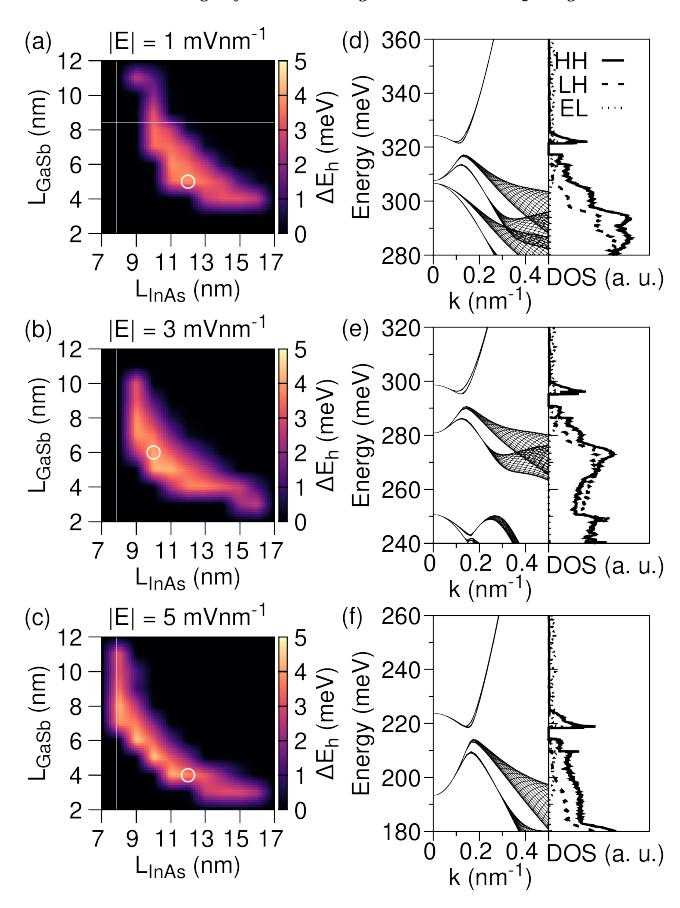


Figure 2. Hybridization gap heatmap of the GaSb/InAs/GaSb SQW as a function of the InAs and GaSb layer sizes. Through (a) to (c) we show the hybridization gaps for several values of external electric field, the open circles indicate the sizes used to plot, through (d) to (f), the band structures and the projected DOSs after the band inversion. The label HH refers to heavy-hole, LH to light-hole and EL to electrons (or conduction band). More specifically, in (a)  $|E| = 1 \,\mathrm{mV}\,\mathrm{nm}^{-1}$ , in (b)  $|E| = 3 \,\mathrm{mV}\,\mathrm{nm}^{-1}$  and in (c)  $|E| = 5 \,\mathrm{mV}\,\mathrm{nm}^{-1}$ . In (d)  $L_{\mathrm{GaSb}} = 5 \,\mathrm{nm}$  and  $L_{\mathrm{InAs}} = 12 \,\mathrm{nm}$ , in (e)  $L_{\mathrm{GaSb}} = 6 \,\mathrm{nm}$  and  $L_{\mathrm{InAs}} = 10 \,\mathrm{nm}$  and in (f)  $L_{\mathrm{GaSb}} = 4 \,\mathrm{nm}$  and  $L_{\mathrm{InAs}} = 12 \,\mathrm{nm}$ . The wave vector k in (d), (e) and (f) is defined as  $k = \sqrt{k_x^2 + k_y^2}$ .

changes the relative energy difference between states on different layers. For positive (negative) applied electric fields, the outer holes states of the left (right) GaSb layer increases in energy while the electron energy level decreases. A trivial band alignment, with electron states having higher energies than holes, may become an inverted alignment for a sufficient large electric field. Further increasing the electric field value may turn this inverted regime system into a deeply inverted regime as in the InAs/GaSb AQW [40, 42].

The deeply inverted regime can be engineered either by finding the right combination of the layer sizes or by an applied electric field. From figure 2(a)-(c), we can identify this regime by choosing a system configuration which is on the verge of becoming gapless. One could also identify it by looking at the

wave vector value where the subbands anticross each other,  $k_c$ . For small magnitudes of the electric field, the hybridization occurs closer to Γ-point and, therefore, the value of  $k_c$  is also smaller, compared to large values of electric field in the same system. In our data, the values vary in the ranges of  $k_c \in [0.1, 0.3] \,\mathrm{nm}^{-1}$  and  $v_F \in [1,4] \times 10^4 \,\mathrm{ms}^{-1}$  and though, GaSb/InAs/GaSb SOW shows a deep hybridization.

Figure 2(d)-(f) present the band structures and the projected DOSs for selected deeply inverted regime SQWs, marked as open circles in figure 2(a)-(c), respectively. The band structures were plotted as functions of all  $k_{\parallel}$  setting  $k = \sqrt{k_x^2 + k_y^2}$  allowing the visualization of features from all directions of the band structures at once. The asymmetries of the valence band become very clear for wave vectors away from  $\Gamma$ -point, showed as the spreading in energy of a given subband. In the inverted regime the largest contribution in the projected DOS near the hybridization gap region is due to the heavy-hole subband. Although the conduction band state should be a linear combination of electrons and light-holes, as explicitly shown in simplified models of topologically protected systems, like the Bernevig-Hughes-Zhang (BHZ) model [59], the light-hole contribution on the valence band is only relevant for wave vectors away from the  $\Gamma$ -point and/or energies well below the hybridization region. This means that in order to correctly describe the low-energy spectrum of such SQW there is no need to include the light-hole band, as it is important for the InAs/GaSb AQW [42, 6], although we need to include the extra heavy-hole band [7].

The effect of the electric field in expelling the lower heavy-hole subbands can be seen in figure 2(d), 2(e) and 2(f). In figure 2(d) both heavy-hole subbands are almost degenerate at  $\Gamma$  with energies close to 310 meV. The spin-splitting of each subband is seen at higher  $k_{\parallel}$ . In fig 2(e), the second heavy-hole appears at around 250 meV and in figure 2(f) it is out of the range. Therefore, in the limit of very large electric fields the system becomes similar to the InAs/GaSb AQW, *i. e.*, the electric field isolates one of the GaSb layers from the GaSb/InAs and simpler models such as the aforementioned BHZ model [59] can describe very accurately the low energy properties of the system.

## Massless Dirac fermions

The investigation of the Dirac cones like energy dispersion and edge states is usually done by using effective models that include a limited number of bands, such as the 4-band BHZ model [59] and other extended BHZ-like models that include extra subbands [6, 7]. The advantage of these models is the number of states included, requiring smaller

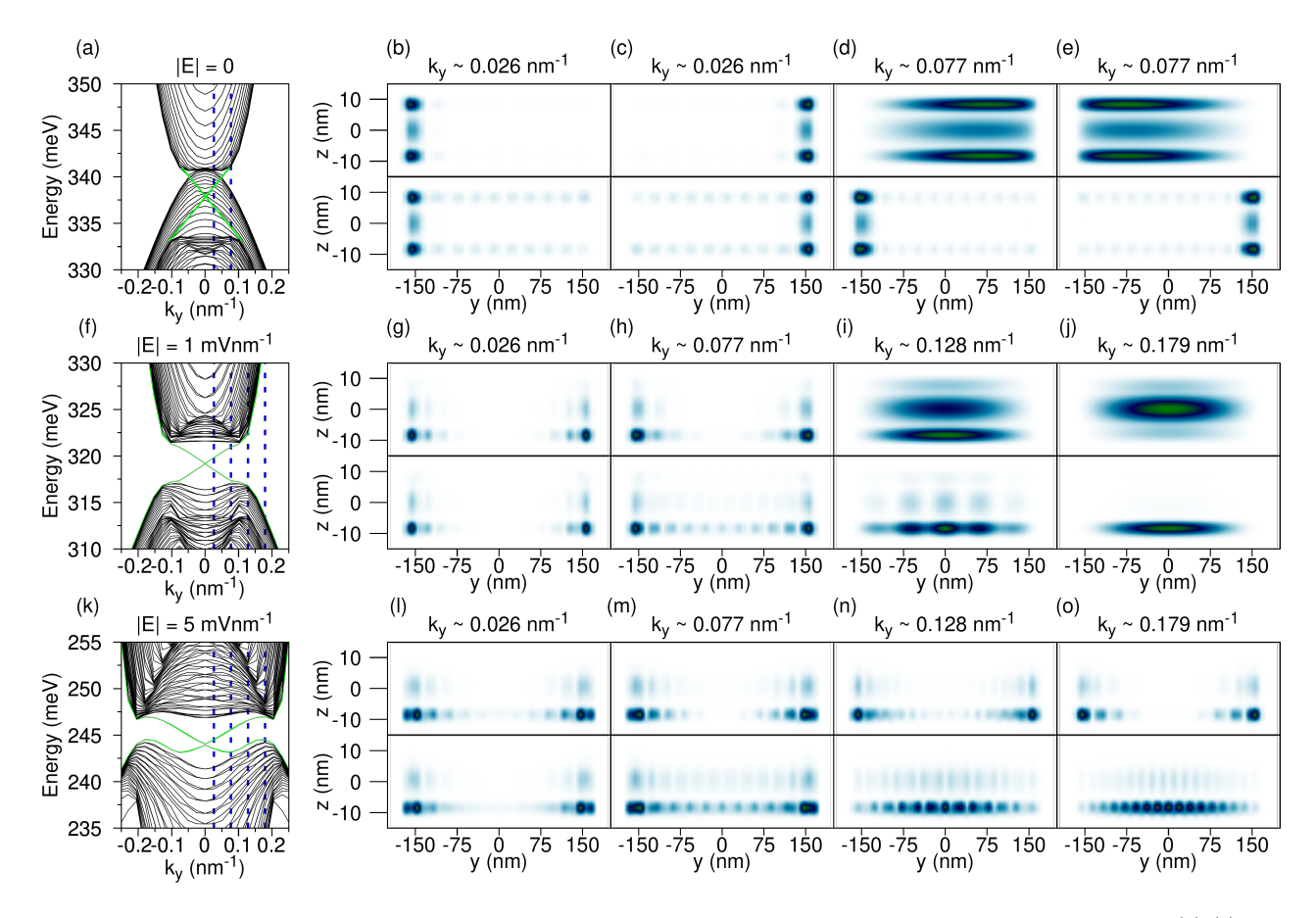


Figure 3. Energy dispersion and edge states probability densities for a  $L_{\text{GaSb}} = 5 \,\text{nm}$  and  $L_{\text{InAs}} = 12 \,\text{nm}$  SQW. (a)-(e) are for E = 0. (f)-(j) are for  $|E| = 1 \,\text{mV}\,\text{nm}^{-1}$ . (k)-(o) are for  $|E| = 5 \,\text{mV}\,\text{nm}^{-1}$ . The green lines in (a), (f) and (k) are guidelines to highlight where the Dirac cone like dispersion is. The blue lines in the same panels show the wave vectors depicted in the right hand panels.

computational resources to be numerically solved. What makes them simpler, in few words, is that symmetry is used to define a basis, with a smaller number of states that describes the essential features of the system in the confinement direction. This basis, composed by states that are linear combinations of components of the original basis specifically tuned to describe the intended few subbands near the gap, is used to generate an effective Hamiltonian that has the confinement direction integrated out and replaced by a set of parameters. The integration that allows to simplify the description is also its major drawback, since the spatial resolution of the probability densities along the quantum well confinement is lost. Here, instead of using the BHZ-like models, we use the full 3D 8-band  $\mathbf{k} \cdot \mathbf{p}$  model, and therefore, we keep the spatial resolution along the quantum well confinement axis.

Analyzing the probability densities one can see that as we increase the momentum,  $k_y$ , they transition from a edge localized state to a sample centered localized state. Another feature is that the edge states are oscillating [6], i. e., they have peaks and

nodes along the y direction, but in general the density presents a very intense peak near the edge and the intensity of the peaks toward the center diminish, forming a tail. In the Supplementary Material we briefly go over the reason why such oscillations are present, a more detailed explanation is given in Ref. [60].

In figure 3(a) the system has a linear energy dispersion band (emphasized by the green line) but it is embedded on the valence subbands, *i. e.*, there is an edge state that connects the conduction band to the second valence band [7]. Although such edge state exists, the system is in a semimetal phase since no overall gap is present. To verify that this embedded linear energy dispersion corresponds to edge states, we plot in figure 3(b)-(e) the probability density of such states, for the conduction band (upper panels) and valence band (lower panels) at  $k_y = 0.026 \,\mathrm{nm}^{-1}$  ((b) and (c)) and at  $k_y = 0.077 \,\mathrm{nm}^{-1}$  ((d) and (e)). Notice first that each state is doubly degenerate in spin. Therefore, in figure 3(b) and 3(c) we plot the probability density of one of the spin components,

while in figure 3(d) and 3(e) we plot the other spin component, for a given wave vector. It is evidently clear that these states are helical edge states since each spin projection is confined along an opposite edge of the slab. Moreover, by using the full 3D  $\mathbf{k} \cdot \mathbf{p}$ description we are able to see that the edge states are symmetric with respect to the InAs layer (central layer), since there is no electric field breaking this symmetry, and are predominantly located into the GaSb layers. For  $k_y = 0.077 \,\mathrm{nm}^{-1}$  the conduction band edge state is still predominantly in the GaSb layer but it is also more spread throughout the slab and does not present oscillations indicating that it is losing its edge state character and is becoming a bulk-like state. The existence of a Dirac cone inside the valence band continuum may be understood as Bound State in the Continuum, or BIC, phenomena [61]. In this specific case a symmetry protect BIC emerges inside the continuum of the valence band due to the presence of a reflection symmetry.

In figure 3(f)-(j) we show the energy dispersion and the probability densities for the same GaSb/InAs/GaSb multilayer with applied electric field of  $|E| = 1 \,\mathrm{mV} \,\mathrm{nm}^{-1}$ . In figure 3(f) we see that the second heavy-hole band is no longer on the same energy range as the Dirac cone like energy dispersion and that it has become very visible and well isolated from the other subbands. The probability densities are shown on figure 3(g)-(j), but now at four distinct wave vector values and its worth noticing that, although we are only showing one of the spin components, they have peaks at both interfaces with opposite spin projections (as it should be for helical edge states) [62]. Since there is an applied electric field, the states are not anymore symmetric with respect to the InAs layer, however they still are predominantly confined on the GaSb layers. The probability densities at  $k_y = 0.026 \,\mathrm{nm}^{-1}$ and  $k_y = 0.077 \,\mathrm{nm}^{-1}$  show the edge states with oscillation and light tails as seen in figure 3(g) and 3(h). As the wave vector increases however, the overall behavior of these oscillations change and the more intense peaks start spreading from the edges to the center of the slabs, as seen in the valence band panel of figure 3(h). Further increasing the wave vector, the oscillations end on the conduction band, even though the state still has a higher confinement on the GaSb layer - but persists on the valence band but now the oscillations are in small number and more intense at the center of the confining potential, as seen in figure 3(i). This mixed state is on the transition from an edge state to a bulk state and we can see that its wave vector is at the point where the Dirac cone dispersion touches the bulk-like energy dispersion. Choosing the wave vector away from the Dirac cone like energy dispersion region, see figure 3(j), the states become bulk-like states in which the conduction band has its peak on the InAs layer and the valence band on the GaSb layer.

A striking feature of some quantum spin Hall systems, such as InAs/GaSb AQW and HgTe/(Hg,Cd)Te QWs, is that it was experimentally observed that they host a robust helical edge state which persists up to an applied magnetic field of several Tesla [3, 4]. This robustness was latter on explained by the burying of the Dirac cone energy dispersion into the valence subbands [6, 5]. Here, we also show that proposed SQW quantum spin Hall system also has such buried Dirac cone, and therefore hosts a robust edge that should persists up to several Tesla. In general, for such feature to be present in the SQW it must be in the deeply inverted regime. Therefore, if a selected system does not present the buried Dirac cone dispersion, a recipe to achieve it is to increase the applied electric field, thus enhancing the inverted regime. In figure 3(k) we can see that by increasing the applied electric field we push the minimal energy difference between the subbands away from the  $\Gamma$ -point (it is at  $0.0 \text{ nm}^{-1}$  in (a), a little below 1.28 $nm^{-1}$  in (f) and close to 0.2  $nm^{-1}$  in (k)), meaning that (k) is on a deeply inverted regime. Focusing on the right panel of figure 3(k), one can see that, indeed, the Dirac cone dispersion was pushed down towards the bulk valence subbands and it is hidden.

In figure 3(l)-(o) we show the probability densities of four selected wave vector values. The behavior as we increase the  $k_y$  value is similar to that we discussed early. The only distinction is that the valence band branch of the Dirac cone dispersion touches the bulk valence bands while inside the hybridization region. This changes the probability densities from a edge localized to bulk like but still with the oscillations, as we can see in figure 3(m)-(o), while the conduction band branch still shows edge localized states.

In summary, the hybridization gap for the GaSb/InAs/GaSb SQW have a similar magnitude as the InAs/GaSb AQW. The presence of an extra heavyhole subband, due to the second GaSb layer, precludes the opening of the hybridization gap and by tuning the layer sizes, the system only presents a semiconductorsemimetal transition. The application of an external electric field is therefore a requirement to open the hybridization gap. Moreover, estimations of  $k_c$  and  $v_F$ indicate that this system is in a deeply inverted regime. By confining along the y direction and analyzing the spatial distribution of the edge states we discovered that they are predominantly confined at the GaSb layer. As we could see, in figure 3, as we increase the applied electric field and enhance the inverted regime, the probability densities become more oscillating and its overall maximum go further to the middle of the confining profile.

## 2.2. InAs/GaSb/InAs multilayer

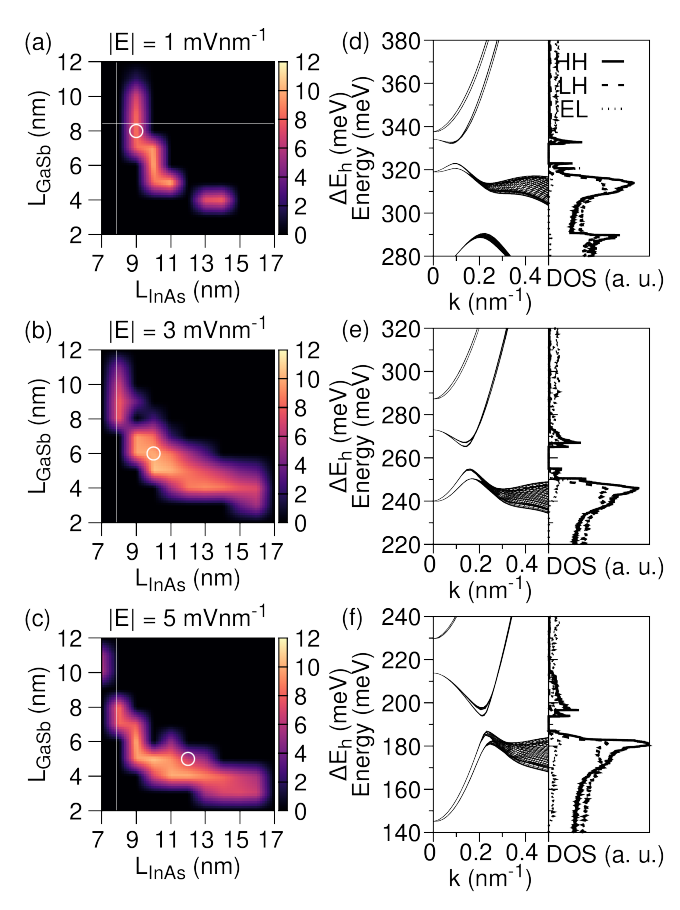


**Figure 4.** Same as figure 2 but in (d)  $L_{\rm GaSb}=8\,{\rm nm}$  and  $L_{\rm InAs}=9\,{\rm nm}$ , in (e)  $L_{\rm GaSb}=6\,{\rm nm}$  and  $L_{\rm InAs}=10\,{\rm nm}$  and in (f)  $L_{\rm GaSb}=5\,{\rm nm}$  and  $L_{\rm InAs}=12\,{\rm nm}$ .

In the InAs/GaSb/InAs configuration, electrons are confined in the lateral wells and the holes inside the central well as seen in figure 1(d). As shown in the Supplementary Material, the semiconductor-semimetal transition occurs as a result of the interaction of the subbands that gradually shifts the top of the valence band away from  $\Gamma$ -point while at the same time the electron subbands penetrates the valence ones. In this section we explore the phase diagram of the InAs/GaSb/InAs SQW.

Figure 4(a)-(c) present heatmaps with the complete phase diagram of the hybridization as a function of  $L_{\rm InAs}$  and  $L_{\rm GaSb}$  for the same three absolute values used in InAs/GaSb/InAs systems:  $|E| = 1\,{\rm mV\,nm^{-1}}$ ,  $|E| = 3\,{\rm mV\,nm^{-1}}$  and  $|E| = 5\,{\rm mV\,nm^{-1}}$ . Similarly to the GaSb/InAs/GaSb SQW, the hybridization gap occurs for distinct values of the layers since the electric field counteracts the effect of the quantum confinement by decreasing (increasing) the energy of the conduction (valence) states. Also similarly to the previous SQW  $k_c \in [0.1, 0.3]\,{\rm nm^{-1}}$  and  $n_c \in [2, 14] \times 10^{11}\,{\rm cm^{-2}}$ . However, since  $\Delta E_h$  is

larger the  $v_F \in [3,9] \times 10^4 \,\mathrm{ms^{-1}}$  meaning that the InAs/GaSb/InAs SQW is not so much in a deep inverted regime compared to InAs/GaSb AQW and GaSb/InAs/GaSb SQW.

Figure 4(d)-(f) presents the band structures and the projected DOSs for selected representative multilayers, marked as open circles in figure 4(a)-(c), respectively. Analogous to the previous case, the asymmetries of the valence band become clear for wave vectors away from  $\Gamma$ -point and are shown as the energy spreading of a given subband and again, in the inverted regime, the largest contribution in the projected DOS near the hybridization gap region is from the heavyhole band. The light-hole contribution is only relevant for wave vectors away from the  $\Gamma$ -point and/or energies well below the hybridization region. This means that in order to correctly describe the low-energy spectrum of such SQW there is no need to include the light-hole band although the need to include one extra electron band [7].

The effect of the electric field in expelling the electron subbands can be seen in figure 4(d)-(f), in which for a small electric field, the second electron subband is less than 10 meV distant from the first and for  $|5| \,\mathrm{mV} \,\mathrm{nm}^{-1}$  is about 20 meV. In the limit of very large electric fields, the system becomes similar to the InAs/GaSb AQW, *i. e.*, the electric field isolates one of the InAs layers from the other GaSb and InAs layers. Therefore, simpler models such as the BHZ model [59] can describe very accurately the low energy properties of the system.

## Massless Dirac fermions

In figure 5(a) we show the band structure for the case without applied electric field. We can see that due to the conduction and valence band hybridization, as discussed in the Supplementary Material, the system shows a very isolated Dirac cone energy dispersion. Figure 5(b)-(e) shows the probability densities of the edge states at four selected wave vector values. Notice that contrary to the previous case, the linear dispersion here is not embedded on the valence subbands and instead it is isolated at the hybridization gap energy region. Only one of the spin components of each state is shown since the other component is its conjugate.

For  $k_y = 0.026 \mathrm{nm}^{-1}$ , the edge states are well confined at the edges of the system and the oscillatory tail towards the middle of the slab have almost zero intensity, as seen in figure 5(b). Moving away, for  $k_y = 0.077 \mathrm{nm}^{-1}$  (figure 5 (c)), the conduction band states have already become bulk-like states with the probability density maximum on the GaSb layer while the valence states are yet confined at the edges. For  $k_y = 0.128 \mathrm{nm}^{-1}$  (figure 5(d)) the states are outside the Dirac cone dispersion region (see figure 5(a)). In this

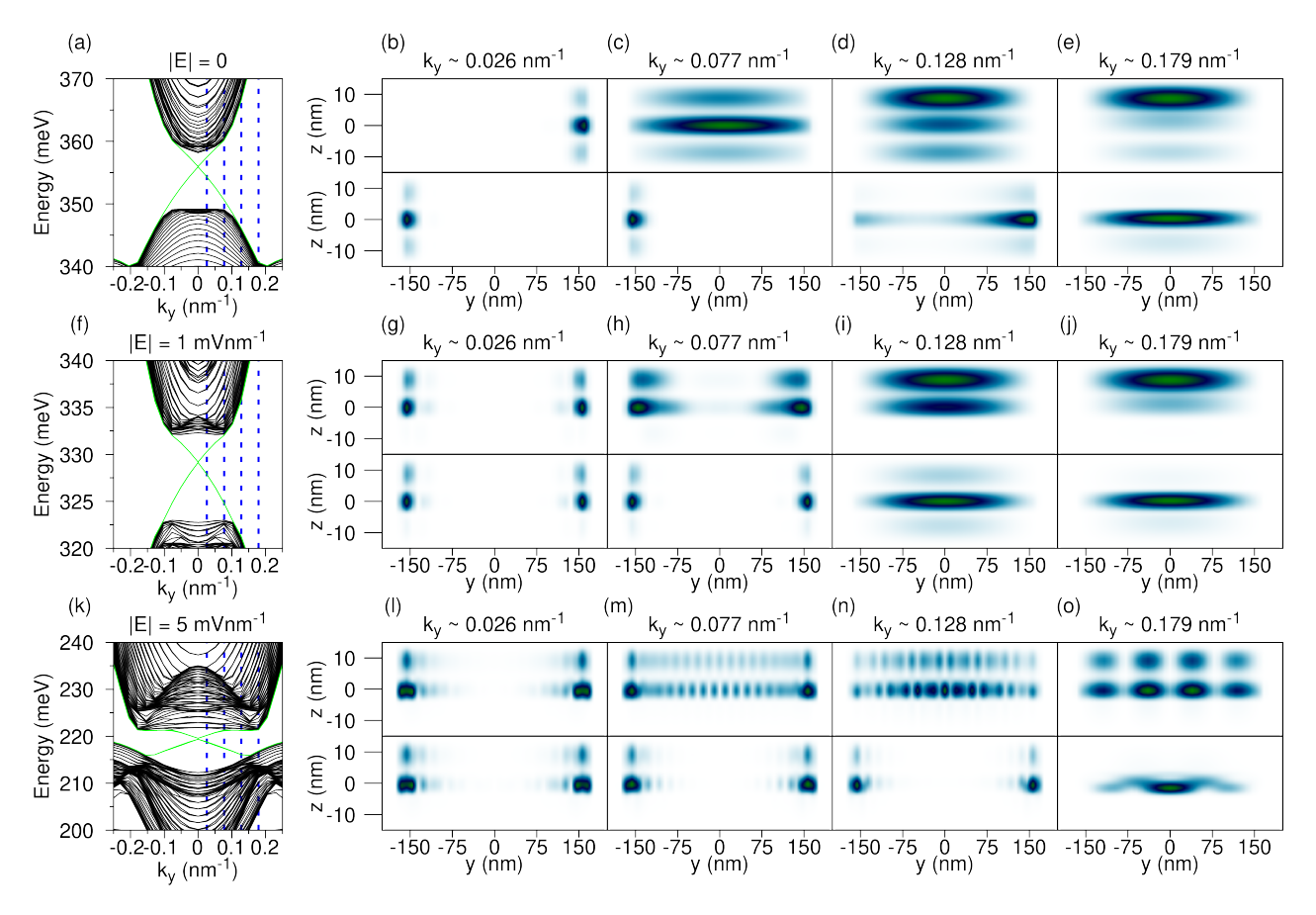


Figure 5. Energy dispersion and edge states probability densities for a  $L_{\rm GaSb}=8\,{\rm nm}$  and  $L_{\rm InAs}=9\,{\rm nm}$  SQW. (a)-(e) are for E=0. (f)-(j) are for  $|E|=1\,{\rm mV\,nm^{-1}}$ . (k)-(o) are for  $|E|=5\,{\rm mV\,nm^{-1}}$ . The green lines in (a), (f) and (k) are guidelines to highlight where the Dirac cone is. The blue lines in the same panels show the wave vectors depicted in the right hand panels.

case, the conduction band state is bulk-like and now mostly confined at the InAs layer while the valence band still shows confinement near the edges but with non-zero probability density all over the slab. Finally for  $k_y = 0.179 \mathrm{nm}^{-1}$ , in figure 5(e), all the states are bulk like, with both conduction and valence states confined at the center of the confining potential.

The application of an external electric field accentuates the edge states features. From the previous section, we know that it pushes the second electron subband away from the hybridization energy range and the  $k_c$  is pushed further away from the  $\Gamma$ -point. Figure 5 (g)-(j) show probability densities for selected wave functions in a system with  $|E| = 1 \,\mathrm{mV} \,\mathrm{nm}^{-1}$ . For  $k_y = 0.026 \,\mathrm{nm}^{-1}$ , the states are very confined at the edges with almost no oscillatory tail towards the center of the slab, as seen in figure 5(g). Figure 5(h) shows that both, conduction and valence band states at  $k_y = 0.077 \,\mathrm{nm}^{-1}$ , are still edge states. However, the conduction band density probability has a nonoscillatory stronger tail towards the center of the slab and both states are more localized in the GaSb region. Moving to  $k_y = 0.128 \,\text{nm}^{-1}$  and  $k_y = 0.179 \,\text{nm}^{-1}$ , we get away from the Dirac cone dispersion region and, indeed, the states becomes bulk-like and conduction band states become localized at one of the InAs regions, as seen in figure 5(i) and 5(j).

The estimations of the Fermi velocities for the InAs/GaSb/InAs SQW,  $v_F \in [3,9] \times 10^4\,\mathrm{ms}^{-1}$ , indicates that its inverted regime is not as deep as the GaSb/InAs/GaSb SQW. Indeed, by analyzing the probability densities of both SQWs we gather that the former has well localized edge states while the latter has edge states with a highly oscillating tail. Moreover, the Fermi velocity is dependent on the hybridization gap and a larger  $\Delta E_h$  (which is the case of InAs/GaAs/InAs) gives a larger velocity, therefore making this a better candidate to host experimentally detect the massless Dirac fermions.

By increasing the applied electric field we can tune the system to a deeply inverted regime, as discussed before, where the Dirac cone becomes buried in the bulk valence subbands. In figure 5(k) we present the energy dispersion showing a distinct case since the top of the valence band is at a finite wave vector away from  $\Gamma$ -point, almost engulfing the conduction band. In such

a situation a hidden Dirac cone is developed. Focusing on the right panel of figure 5(k) one indeed see that the Dirac cone like energy dispersion is hidden.

Figure 5(1)-(o) show the probability densities of four selected wave vector values. For  $k_y = 0.026 \,\mathrm{nm}^{-1}$ the edge states are very confined at the edges with a slightly oscillating tail, as seen in figure 5(1). As the wave vector increases, the oscillations of the conduction band edge state are accentuated, but the valence band edge state remains unchanged, as seen in figure 5(m). In figure 5(n), for  $k_y = 0.128 \,\mathrm{nm}^{-1}$ , the conduction band edge state has switched to a more bulk-like state with a higher probability to be found in the center but still with an oscillating pattern, while the valence band is still well localized at the edge. Moving to  $k_y = 0.179 \,\mathrm{nm}^{-1}$ , see 5(o), we are still inside the hybridization region, although both conduction and valence states had acquired a more bulk like shape they are not yet fully bulk states.

In summary, the hybridization gap for the InAs/GaSb/InAs SQW is about 12 meV and larger than both GaSb/InAs/GaSb SQW and InAs/GaSb AQW and the estimation of  $k_c$  and  $v_F$  indicates that the system is not so deep inverted as its counterparts. By confining along the y direction and analyzing the spatial distribution of the edge states it is shown that they are predominantly confined at the GaSb layer. As we could see, in figure 5, the edge states are very localized at the edges with very small oscillating tail, if any. By increasing the electric field we could transition the system to a deeply inverted one with a hidden Dirac cone.

#### 3. Modeling details

To correctly account for the hybridization of the conduction and valence bands an accurate description of the valence band states is needed, specially for the heavy- and light-hole states. The usual 8-band Kane model [45] is not adequate for this description since it gives the wrong value for the effective mass of the heavy-hole states in certain materials [63]. In this work we used the 8-band  $\mathbf{k} \cdot \mathbf{p}$  model including the conduction band states, the three valence bands, the explicit coupling between them and the Luttinger corrections for the effective masses [44, 46, 47]. This model has been successfully applied in describing the electronic and spintronic properties of low dimensional semiconductor for decades [51, 64, 65, 66, 67, 48], including the InAs/GaSb AQWs. [6, 5, 68, 69, 70, 71, 72, 73, 74, 75, 76, 77]

The  $\mathbf{k} \cdot \mathbf{p}$  model describes a bulk material around a high symmetry point, usually the  $\Gamma$ -point, where the physics of interest takes place. To correctly describe it, a parametrization of the matrix elements

among the basis states (Bloch functions) is derived using Group Theoretical methods. To describe a heterostructure, as a QW, we apply the envelope function approximation [49, 63], that defines the total wave function of a state of the system as a continuous and slowly varying function, called the envelope function, that is weighted by the Bloch's function of each material. The quantum confinement along the growth direction essentially means that we have to make the substitution  $k_z \rightarrow -i\frac{\partial}{\partial z}$ . This approach results in a system of coupled linear differential equations. This system is solved by applying the plane wave expansion, using the Fourier transformations—using 40 planes waves which suffices to achieve energy convergence in our calculations. The method is well described in our previous works [64, 48 We solve the final matrix Hamiltonian by direct diagonalization methods using the MAGMA [78] suite which implements the LAPACK routines in a multicore + GPU (graphical processing unit) computational environment.

The parameters used in the 8-band  $\mathbf{k} \cdot \mathbf{p}$  model were extracted from Ref. [79]. It is know that solution of narrow gap semiconductors is plagued with spurious solutions and to avoid it we apply a renormalization of the Kane interband momentum matrix element, P, as suggested by Ref. [80],

$$P^{2} = \left(\frac{m_{0}}{m_{c}} - 1\right) \frac{E_{g} \left(E_{g} + \Delta\right)}{E_{g} + \frac{2}{3}\Delta} \frac{\hbar^{2}}{2 m_{0}} \tag{1}$$

where we set  $\frac{m_0}{m_c} = 1$  with  $E_g$  being the gap energy and  $\Delta$  the spin-orbit splitting energy. With the new P we then calculate the new corrected Luttinger parameters according to

$$\tilde{\gamma_1} = \gamma_1 - \frac{E_P}{3E_g}$$

$$\tilde{\gamma_2} = \gamma_2 - \frac{E_P}{6E_g}$$

$$\tilde{\gamma_3} = \gamma_3 - \frac{E_P}{6E_g}$$

$$A = \frac{1}{m_e^*} - \left(\frac{E_g + \frac{2}{3}\Delta_{SO}}{E_g + \Delta_{SO}}\right) \frac{E_P}{E_g}$$
where  $E_P = \frac{2m_0}{E_P} P^2$ . (2)

#### 4. Conclusion

In this manuscript we have explored the electric control of the topological phase transition in GaSb/InAs/GaSb and InAs/GaSb/InAs symmetric multilayers and the spatial distribution of the edge states probability density using a full 3D 8-band  $\mathbf{k} \cdot \mathbf{p}$  method.

We have calculated the full hybridization gap phase diagram by varying the layer size and applied electric field. We have shown that the hybridization gap for the GaSb/InAs/GaSb SQW have values around 5 meV that are very similar to the InAs/GaSb AQW, while for InAs/GaSb/InAs SQW is about 12 meV. In both systems the hybridization occurs at similar values of wave vector  $k_c \in [0.1, 0.3] \, \mathrm{nm}^{-1}$ , therefore the InAs/GaSb/InAs SQW having a large hybridization gap will also have a larger Fermi velocity. Ultimately, this means that the edge states of the InAs/GaSb/InAs SQW are less interacting with the bulk bands.

By applying a weak confinement along the y direction and analyzing the spatial distribution of the edge states, we verified that they are predominantly confined at the GaSb layer. By increasing the electric field we tune the system to a deeply inverted regime with a hidden/buried Dirac cone like energy dispersion having highly oscillating probability densities with large tails towards the bulk. Although this feature is present in both multilayers, the InAs/GaSb/InAs SQW due to its large hybridization gap, suppress it, and therefore is suggested as the better option to explore the rich physics offered by the quantum spin Hall

Departing from the two systems under consideration, we have unambiguously demonstrated the relevance of the InAs/GaSb three-layer heterostructures. Being a platform extremely tunable, they can be used as a playground to further expand out scientific knowledge of topics ranging from many-body interactions [25, 27, 29] – tuning  $\Delta E_h$  to very small values – to quantum computing with Majorana fermions [52, 53] – tuning  $\Delta E_h$  to large values.

## Acknowledgments

This work has been partially supported by CAPES (CsF - grant No. 88881.068174/2014-01 and PNPD - grant No. 88882.306206/2018-01) and PLAF / SBF / CNPq. The first author thanks the LCCA for computational resources, D. R. Candido and P. E. Faria Junior for useful insights and discussion. L. D-C gratefully acknowledge the hospitality of IFSC-USP.

#### References

- [1] Qi X L and Zhang S C 2011 Reviews of Modern Physics 83(4) 1057–1110
- [2] Hasan M Z and Kane C L 2010 Reviews of Modern Physics 82(4) 3045–3067
- [3] Du L, Knez I, Sullivan G and Du R R 2015 Physical Review Letters 114 096802
- [4] Ma E Y, Calvo M R, Wang J, Lian B, Mühlbauer M, Brüne C, Cui Y T, Lai K, Kundhikanjana W, Yang Y et al. 2015 Nature Communications 6 7252
- [5] Skolasinski R, Pikulin D I, Alicea J and Wimmer M 2017 ArXiv e-prints (Preprint 1709.04830)
- [6] Li C A, Zhang S B and Shen S Q 2018 Physical Review B 97 045420

- [7] Krishtopenko S S and Teppe F 2018 Science Advances 4  $^{4-7}$
- [8] Sakaki H, Chang L L, Ludeke R, Chang C A, Sai-Halasz G A and Esaki L 1977 Applied Physics Letters 31 211– 213
- [9] Sai-Halasz G, Esaki L and Harrison W 1978 Physical Review B  ${\bf 18}$  2812
- [10] Ting D Z Y, Collins D A, Yu E T, Chow D H and McGill T C 1990 Applied Physics Letters 57 1257–1259
- [11] Chow D H, Miles R H, Schulman J N, Collins D A and McGill T C 1991 Semiconductor Science and Technology 6 C47
- [12] Lakrimi M, Khym S, Nicholas R, Symons D, Peeters F, Mason N and Walker P 1997 Physical Review Letters 79 3034
- [13] Yang M, Yang C, Bennett B and Shanabrook B 1997 Physical Review Letters 78 4613
- [14] Nicholas R, Lakrimi M, Khym S, Mason N, Poulter A, Vaughan T, Walker P, Maude D, Portal J, Symons D et al. 1998 Physica B: Condensed Matter 256 207–214
- [15] Ting D Z Y and Cartoixà X 2002 Applied Physics Letters 81 4198–4200
- [16] Kroemer H 2004 Physica E: Low-dimensional Systems and Nanostructures 20 196–203
- [17] Liu C, Hughes T L, Qi X L, Wang K and Zhang S C 2008 Physical Review Letters 100 236601
- [18] Knez I, Du R R and Sullivan G 2011 Physical Review Letters 107 136603
- [19] Knez I, Du R R and Sullivan G 2012 Physical Review Letters 109(18) 186603
- [20] Suzuki K, Harada Y, Onomitsu K and Muraki K 2013 Physical Review B 87 235311
- [21] Nichele F, Pal A N, Pietsch P, Ihn T, Ensslin K, Charpentier C and Wegscheider W 2014 Physical Review Letters 112 036802
- [22] Spanton E M, Nowack K C, Du L, Sullivan G, Du R R and Moler K A 2014 Physical Review Letters 113 026804
- [23] Marlow T, Cooper L, Arnone D, Patel N, Whittaker D, Linfield E, Ritchie D and Pepper M 1999 Physical Review Letters 82 2362
- [24] Naveh Y and Laikhtman B 1996 Physical Review Letters 77 900
- [25] Pikulin D and Hyart T 2014 Physical Review Letters 112 176403
- [26] Pribiag V S, Beukman A J, Qu F, Cassidy M C, Charpentier C, Wegscheider W and Kouwenhoven L P 2015 Nature Nanotechnology 10 593
- [27] Li T, Wang P, Fu H, Du L, Schreiber K A, Mu X, Liu X, Sullivan G, Csáthy G A, Lin X and Du R R 2015 Physical Review Letters 115 136804
- [28] Du L, Li T, Lou W, Wu X, Liu X, Han Z, Zhang C, Sullivan G, Ikhlassi A, Chang K and Du R r 2017 Physical Review Letters 119 056803
- [29] Du L, Li X, Lou W, Sullivan G, Chang K, Kono J and Du R R 2017 Nature Communications 8 1971
- [30] Mueller S, Pal A N, Karalic M, Tschirky T, Charpentier C, Wegscheider W, Ensslin K and Ihn T 2015 Physical Review B 92 081303
- [31] Karalic M, Mueller S, Mittag C, Pakrouski K, Wu Q, Soluyanov A A, Troyer M, Tschirky T, Wegscheider W, Ensslin K et al. 2016 Physical Review B 94 241402
- [32] Nichele F, Suominen H J, Kjaergaard M, Marcus C M, Sajadi E, Folk J A, Qu F, Beukman A J, de Vries F K, van Veen J et al. 2016 New Journal of Physics 18 083005
- [33] Nguyen B M, Kiselev A A, Noah R, Yi W, Qu F, Beukman A J, de Vries F K, van Veen J, Nadj-Perge S, Kouwenhoven L P et al. 2016 Physical Review Letters 117 077701
- [34] Akiho T, Couëdo F, Irie H, Suzuki K, Onomitsu K and Muraki K 2016 Applied Physics Letters 109 192105

- [35] Kononov A, Kostarev V, Semyagin B, Preobrazhenskii V, Putyato M, Emelyanov E and Deviatov E 2017 Physical Review B 96 245304
- [36] Mueller S, Mittag C, Tschirky T, Charpentier C, Wegscheider W, Ensslin K and Ihn T 2017 Physical Review B 96 075406
- [37] Kim M, Kim C H, Kim H S and Ihm J 2012 Proceedings of the National Academy of Sciences 109 671–674
- [38] Liu Q, Zhang X, Abdalla L, Fazzio A and Zunger A 2015 Nano letters 15 1222–1228
- [39] Pan H, Wu M, Liu Y and Yang S A 2015 Scientific reports 5 14639
- [40] Qu F, Beukman A J, Nadj-Perge S, Wimmer M, Nguyen B M, Yi W, Thorp J, Sokolich M, Kiselev A A, Manfra M J et al. 2015 Physical Review Letters 115 036803
- [41] Suzuki K, Harada Y, Onomitsu K and Muraki K 2015 Physical Review B 91 245309
- $[42]\,$  Hu L H, Liu C X, Xu D H, Zhang F C and Zhou Y 2016 Physical Review B  ${\bf 94}$  045317
- [43] Qi J, Li X and Qian X 2016 Applied Physics Letters 108 253107
- [44] Luttinger J and Kohn W 1955 Physical Review 97 869
- [45] Kane E O 1966 Physics of III-V compounds (New York: Academic Press) v. 1
- [46] Enderlein R and Horing N J 1997 Fundamentals of semiconductor physics and devices (World Scientific)
- [47] Winkler R 2003 Spin-orbit Coupling Effects in Two-Dimensional Electron and Hole Systems (Physics and Astronomy Online Library no 191) (Springer)
- [48] Campos T, Faria Junior P E, Gmitra M, Sipahi G M and Fabian J 2018 Physical Review B 97 245402
- [49] Burt M 1999 Journal of Physics: Condensed Matter 11 53
- [50] Ehrhardt M and Koprucki T 2014 Multi-band Effective Mass Approximations: Advanced Mathematical Models and Numerical Techniques vol 94 (Springer)
- [51] Sipahi G M, Enderlein R, Scolfaro L M R and Leite J R 1996 Physical Review B 53(15) 9930–9942
- [52] Fatin G L, Matos-Abiague A, Scharf B and Žutić I 2016 Physical Review Letter 117(7) 077002
- [53] Matos-Abiague A, Shabani J, Kent A D, Fatin G L, Scharf B and Žutić I 2017 Solid State Communications 262 1 - 6
- [54] Krishtopenko S S, Ruffenach S, Gonzalez-Posada F, Boissier G, Marcinkiewicz M, Fadeev M A, Kadykov A M, Rumyantsev V V, Morozov S V, Gavrilenko V I, Consejo C, Desrat W, Jouault B, Knap W, Tournié E and Teppe F 2018 Physical Review B 97(24) 245419
- [55] Krishtopenko S S, Desrat W, Spirin K E, Consejo C, Ruffenach S, Gonzalez-Posada F, Jouault B, Knap W, Maremyanin K V, Gavrilenko V I, Boissier G, Torres J, Zaknoune M, Tournié E and Teppe F 2019 Physical Review B 99(12) 121405
- [56] Arias-Laso S and Diago-Cisneros L 2012 Physica E: Lowdimensional Systems and Nanostructures 44 1730 – 1741
- [57] Tsay S F, Chiang J C, Chau Z M and Lo I 1997 Physical Review B  $\bf 56$  13242–13251
- [58] Sandoval M A T, Campos T and Sipahi G M 2017 Tunable band gap inversion in broken gap quantum wells Proceedings of Brazilian Workshop on Semiconductor Physics (Galoa)
- [59] Bernevig B A, Hughes T L and Zhang S C 2006 Science 314 1757–1761
- [60] Erlingsson S I and Egues J C 2015 Phys. Rev. B 91(3) 035312
- [61] Hsu C W, Zhen B, Stone A D, Joannopoulos J D and Soljačić M 2016 Nature Reviews Materials 1 16048
- $[62]\;$  Budagosky J A 2017 Physical Review B  ${\bf 96}\;115443$
- [63] Bastard G 1988 Wave mechanics applied to semiconductor heterostructures (Les Éditions de Physique)
- [64] Rodrigues S C P, Scolfaro L M R, Leite J R and Sipahi G M

- 2000 Applied Physics Letters 76 1015–1017
- [65] Rodrigues S C P, Scolfaro L M R, Leite J R, da Cunha Lima I C, Sipahi G M and Boselli M A 2004 Physical Review B 70(16) 165308
- [66] Faria Junior P E and Sipahi G M 2012 Journal of Applied Physics 112 103716
- [67] Cuan R and Diago-Cisneros L 2015 EPL (Europhysics Letters) 110 67001
- [68] Halvorsen E, Galperin Y and Chao K 2000 Physical Review  $B~{\bf 61}~16743$
- [69] Zakharova A, Yen S and Chao K A 2002 Physical Review B 66 085312
- [70] Lapushkin I, Zakharova A, Yen S and Chao K A 2004 Journal of Physics: Condensed Matter 16 4677
- [71] Andlauer T and Vogl P 2009 Physical Review B 80 035304
- [72] Hong B, Rybchenko S, Itskevich I, Haywood S, Intartaglia R, Tasco V, Raino G and De Giorgi M 2009 Physical Review B 79 165323
- [73] Li J, Yang W and Chang K 2009 Physical Review B 80 035303
- [74] Xu W, Li L, Dong H, Gumbs G and Folkes P 2010 Journal of Applied Physics 108 053709
- [75] Beukman A J, De Vries F K, Van Veen J, Skolasinski R, Wimmer M, Qu F, De Vries D T, Nguyen B M, Yi W, Kiselev A A et al. 2017 Physical Review B 96 241401
- [76] Ndebeka-Bandou C and Faist J 2017 Physical Review B 95 045107
- [77] Jiang Y, Thapa S, Sanders G, Stanton C, Zhang Q, Kono J, Lou W, Chang K, Hawkins S, Klem J et al. 2017 Physical Review B 95 045116
- [78] Dongarra J, Gates M, Haidar A, Kurzak J, Luszczek P, Tomov S and Yamazaki I 2014 Accelerating numerical dense linear algebra calculations with gpus Numerical Computations with GPUs (Springer) pp 3–28
- [79] Vurgaftman I and Meyer J R 2003 Journal of Applied Physics 94 3675–3696
- [80] Foreman B A 1997 Physical Review B 56 R12748